# TITLE PAGE

## Citation Format:

**A. Dalla Mora, L. Di Sieno, E. Ferocino, E. Conca, V. Sesta, M. Buttafava, F. Villa, F. Zappa, D. Contini, A. Torricelli, P. Taroni, A. Tosi, A. Pifferi, "Fast-Gated Digital Silicon Photomultiplier Maximizes Light Harvesting and Depth Sensitivity in Time-Domain Diffuse Optics," in Advances in instrumentation and technology I, Optics InfoBase Conference Papers: ES1B.3, 2021. ISBN: 9781557528209. European Conference on Biomedical Optics 2021 (ECBO), 20-24 June 2021.**

## DOI abstract link:

**https://www.osapublishing.org/abstract.cfm?uri=ECBO-2021-ES1B.3**

# Fast-Gated Digital Silicon Photomultiplier Maximizes Light Harvesting and Depth Sensitivity in Time-Domain Diffuse Optics

**Alberto Dalla Mora*[a], Laura Di Sieno[a], Edoardo Ferocino[a], Enrico Conca[b], Vincenzo Sesta[b], Mauro Buttafava[b], Federica Villa[b], Franco Zappa[b], Davide Contini[a], Alessandro Torricelli[a,c], Paola Taroni[a,c], Alberto Tosi[b], Antonio Pifferi[a,c]**

[a]*Politecnico di Milano, Dipartimento di Fisica, Piazza Leonardo da Vinci 32, 20133 Milano, Italy;*
[b]*Politecnico di Milano, Dipartimento di Elettronica, Informazione e Bioingegneria, Piazza Leonardo da Vinci 32, 20133 Milano, Italy;*
[c]*Consiglio Nazionale delle Ricerche, Istituto di Fotonica e Nanotecnologie, Piazza Leonardo da Vinci 32, 20133 Milano, Italy;*
**alberto.dallamora@polimi.it*

**Abstract:** We show both on phantoms and *in-vivo* the full potential of fast time-gated acquisitions exploiting an innovative custom-developed digital silicon photomultiplier, overcoming consolidated limitations showed by single-photon avalanche diodes linked to their small sensitive area. 

## 1. Introduction

Time-domain diffuse optics (TDDO) is an emerging laser-based technique able to non-invasively probe highly scattering media [1], such as biological tissues, down to a depth of few centimeters when a reflectance geometry is employed [2]. In this configuration, pulsed light is injected and collected, at a certain distance $\rho$ between the two points, on the same side of the sample under investigation. A time-resolved single-photon detector coupled with time-correlated single-photon counting (TCSPC) electronics is employed to reconstruct the distribution of time of flight (TOF) of backscattered photons, which encodes in its shape the information about the probed medium [2]. Further, the TOF of detected photons encodes the average investigated depth: late photons are those bringing information about deeper structures [3].

The advantages of a fast time-gated detection scheme (*i.e.*, physically enabling the detector only during a well delimited time-window) have been proved for TDDO [4]. In particular, thanks to the rejection of scarcely diffused early-photons, this approach extends the dynamic range of the measurement by orders of magnitude [4], thus also allowing to decrease the distance $\rho$. This is particularly interesting as the amount of signal collected at any time $t$ after the laser injection time $t_0$ strongly decreases with the distance from the injection point. However, the real experimental advantage introduced by this approach was limited, as the fast-gating approach has been implemented in the last decade only by using single-photon avalanche diodes (SPADs) [4] with active areas from ~80 μm$^2$ [5] up to ~31400 μm$^2$ [6]. In parallel developments, TDDO benefitted from the introduction of analog silicon photomultipliers (SiPMs) [7], which maximized the light harvesting efficiency thanks to their wide active area (few mm$^2$) and the possibility to operate in direct contact with the tissue under investigation. However, analog SiPMs cannot be time-gated like SPADs, thus they have to be used in configurations with a large distance $\rho$ to avoid the saturation of the acquisition electronics [4,7], thus lowering the intensity of the light eventually collected.

In this work, we present the validation on phantoms and preliminary *in-vivo* tests of a TDDO system based on a custom-designed fast-gated digital SiPM (FG-dSiPM), with active area > 8.6 mm$^2$, bringing together advantages of the large collection area (for light harvesting) and the time-gating feature (for small source-detector separations). The device is divided into 3456 SPADs, 64 of which are partially covered by a metal shield to reduce their active area down to ~20 μm$^2$ (16 SPADs), 79 μm$^2$ (16 SPADs), 314 μm$^2$ (16 SPADs) or 1256 μm$^2$ (16 SPADs). The other 3392 SPADs feature an active area of ~2554 μm$^2$ each. Each SPAD can be separately enabled/disabled in order to increase the detector dynamic range. A full description of this detector is reported in [8].

## 2. Materials and Methods

The experimental setup is composed by: i) a pulsed laser source at a wavelength of 670 nm (LDH P C 670M, Picoquant GmbH) operating at 40 MHz repetition rate, ii) a variable optical attenuator to set the photon counting rate, iii) a black neoprene probe embedding a custom printed circuit board managing the FG-dSiPM (shielded by a glass window) and the laser injection fiber (at $\rho$ = 2.5 cm), in contact with the sample under measurement, iv) a TCSPC board (SPC-130, Becker and Hickl GmbH) hosted inside a personal computer. The instrument response

function of the system, acquired with time-gated modality [4], resulted to have a full-width at half maximum of 280-360 ps, depending on the amount of area enabled, and a dynamic range of more than 5 decades (reported in [9]).

The system has been tested against relevant figures of merit (FoMs) defined by widely adopted characterization protocols, namely, BIP and NEUROPT [2].

The responsivity is a FoM defined in the BIP protocol to quantify the efficiency of the detection chain in detecting scattered light and was here measured to evaluate our detection chain performance.

The sensitivity to deep perturbations was assessed using two FoMs defined in the NEUROPT protocol, namely, contrast (C) and contrast-to-noise ratio (CNR). For this test, a liquid phantom was prepared as described in [9], with standard optical properties at 670 nm (absorption coefficient $\mu_a$ = 0.1 cm$^{-1}$, reduced scattering coefficient $\mu'_s$ = 10 cm$^{-1}$). A totally absorbing perturbation equivalent to a $\Delta\mu_a$ = 0.16 cm$^{-1}$ over 1 cm$^3$ was set at different depths in the phantom, between the injection and collection points. The detector gating window (7 ns width) was delayed with respect to $t_0$ up to the latest delay allowing a photon count rate of 1 million counts per second (Mcps) at full laser power on the sample (*i.e.*, about 5.5 mW, with attenuator fully open). The measurement (acquisition time = 1 s) was repeated for different amounts of enabled active area. C and CNR were evaluated inside a 400 ps time window chosen at a delay along the distribution of TOF that maximized the penetration depth.

As a preliminary *in-vivo* validation, the system was tested in measuring the motor cortex activation in the C3 position (10–20 reference system) on three healthy volunteers performing a standard motor protocol (finger tapping exercise, done with right and left hands, alternatively, with 20 s baseline, 20 s task, 20 s recovery, repeated 5 times). The Ethical Committee of Politecnico di Milano approved the protocol. The study was conducted in agreement with the Declaration of Helsinki. Again, the detector gating window was delayed up to the latest time allowing a photon count rate of 1 Mcps. The measurement (acquisition time = 1 s) was taken by enabling about 5 mm$^2$ of active area, which resulted the best compromise between the signal level and the dynamic range. The C was evaluated inside a 400 ps time window chosen at a delay along the distribution of TOF that maximized the number of photon counts. As a reference case, the average of measurements taken between 5 s and 10 s was considered for each of the 5 blocks of repetitions. The folding average and standard deviation of the 5 repetitions were then computed.

### 3. Results, Discussion and Conclusions

The responsivity at 670 nm resulted to be 1.74·10$^{-6}$ m$^2$sr, a value that is at least 2 orders of magnitude higher than that of any other gated SPAD reported so far in the literature.

Results of the NEUROPT tests are presented in Fig. 1. Assuming as criteria for detectability a contrast > 1% and a CNR > 1, we shaded in grey the regions of the graph where perturbation cannot be detected. As expected, the large area had higher impact on the CNR, which was higher than 1 down to a depth of 42.5 mm (at 8.67 mm$^2$). However, the large collection area also permitted to achieve statistical relevance of photon counts arriving at later delays, thus also increasing the C at deeper positions and achieving its detectability down to a depth of 37.5 mm.

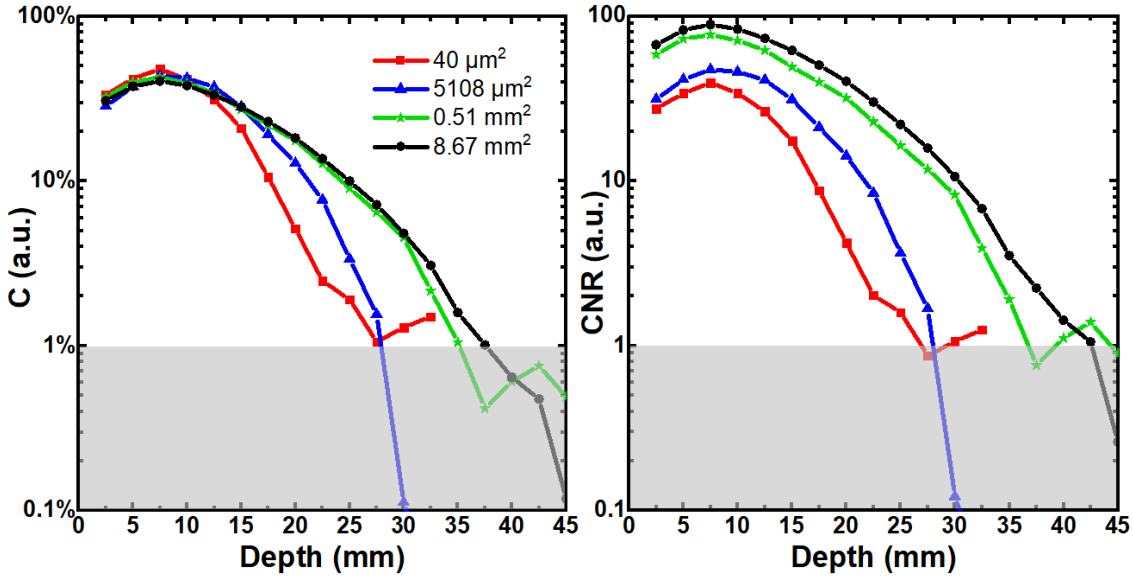


Fig. 1. Contrast C (left) and contrast-to-noise ratio CNR (right) produced by an absorbing perturbation ($\Delta\mu_a$ = 0.16 cm$^{-1}$) set at various depths in the phantom, for different amounts of enabled active areas (colors).

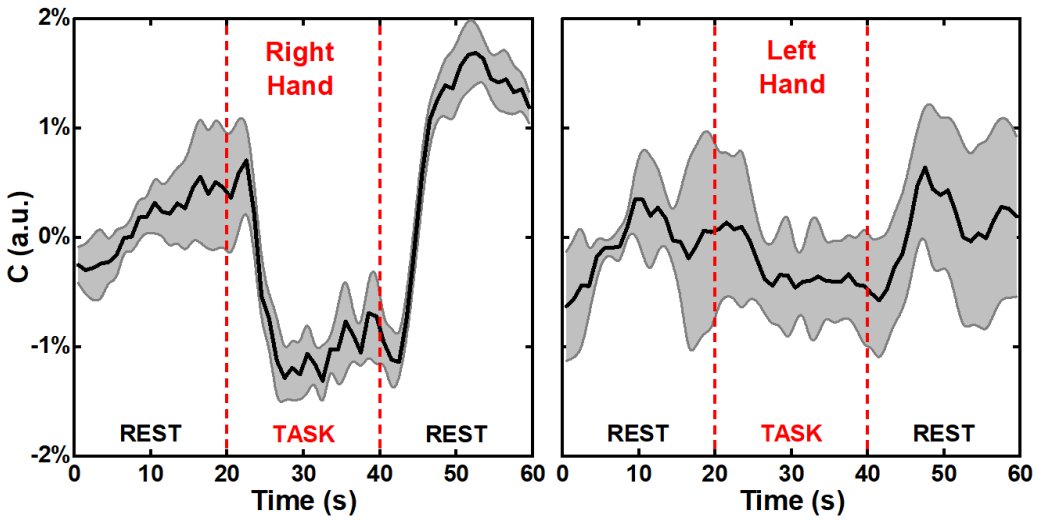


Fig. 2. Contrast C recorded on the motor cortex of a healthy volunteer during a finger tapping exercise performed with the right/left hand. The gray areas represent the standard deviation across different task repetitions.

To the best of our knowledge, this extends the depth sensitivity of time-gated systems reported so far in the literature by about 1 cm. This conclusion is supported by the use of standardized conditions for the evaluation of this FoM.

*In-vivo* results for one subject are reported in Fig. 2. The vertical red bars delimit the timing of the task. The black solid lines represent the folded average of the C across the 5 task repetitions. The grey shadows represent the standard deviation between different repetitions. As shown, the contralateral activation was clear, while negligible ipsilateral activation is detected (as expected). Results on other volunteers (not shown here) were comparable.

In conclusion, thanks to the adoption of a custom FG-dSiPM, this work demonstrated the possibility to achieve time-gated single-photon detection with suitable performance for time-domain diffuse optics applications with active areas at least 300 times wider than that of any other previously reported system based on time-gated SPADs, with advantages in terms of light harvesting efficiency and depth of penetration inside scattering media. The preliminary *in-vivo* validation suggests the suitability of the system for brain functional imaging applications.

## 4. Acknowledgements

The research leading to these results has received partial funding from the European Union's Horizon2020 research and innovation program under project SOLUS: "Smart Optical Laser and Ultrasound Diagnostics of Breast Cancer" (https://www.solus-project.eu). The project is an initiative of the Photonics Public Private Partnership.

## 5. References

[1] T. Durduran, R. Choe, W.B. Baker, A.G. Yodh, "Diffuse optics for tissue monitoring and tomography," Rep Prog Phys **73,** 076701 (2010).

[2] A. Pifferi et al., "New frontiers in time-domain diffuse optics, a review," Biomed Opt **21,** 091310 (2016).

[3] J. Steinbrink et al., "Determining changes in NIR absorption using a layered model of the human head," Phys Med Biol **46,** 879-896 (2001).

[4] A. Dalla Mora, L. Di Sieno, R. Re, A. Pifferi, D. Contini, "Time-gated single-photon detection in time-domain diffuse optics: A review," Appl Sci **10,** 1101 (2020).

[5] S. Saha Y. Lu, S. Weyers, M. Sawan, F. Lesage, "Compact fast optode-based probe for single-photon counting applications," IEE Photon Technol Lett **30,** 1515–1518 (2018).

[6] D. Contini et al., "Effects of time-gated detection in diffuse optical imaging at short source-detector separation," J Phys D (Appl Phys) **48,** 045401 (2015).

[7] A. Dalla Mora et al., "The SiPM revolution in time-domain diffuse optics," Nucl Instrum Methods **978,** 164411 (2020).

[8] E. Conca et al., "Large-area fast-gated digital SiPM with integrated TDC for portable and wearable time domain NIRS," IEEE J Solid St Circ **55,** 3097-3111 (2020).

[9] L. Di Sieno et al., "Time-domain diffuse optics with 8.6 mm$^2$ fast-gated SiPM for extreme light harvesting efficiency," Opt Lett **46,** 424-427 (2021).